Microphase transitions of block copolymer/nanorod composites under shear flow

Linli He,[ab] Zhangquan Pan,[a] Linxi Zhang*[a] and Haojun Liang[c]

Received 21st July 2010, Accepted 19th October 2010
DOI: 10.1039/c0sm00703j

The shear-induced reorientations and phase transitions of symmetric diblock copolymer/nanorod nanocomposites subjected to steady shear flow, are systematically investigated *via* dissipative particle dynamics (DPD) simulation method. Both selective and nonselective nanorods (NRs) are considered, with low and high NRs concentrations. To preserve lamellar morphology in the nanocomposites, the NRs concentration is controlled below 15%. The final morphologies of nanocomposites depend on the interplay between NRs and diblock copolymers (DBCPs) under shear flow. The cooperatively induced microphase structures include lamellar (parallel, diagonal and perpendicular alignment), ribbon and cylindrical phases. The presence of anisotropic NRs not only delays or advances the shear-induced transition in lamellae orientation, but also induces the phase transitions by changing the effective composition of the copolymers (f_{eff}) in nanocomposites. Meanwhile, the low viscosity in the perpendicular lamellae of DBCPs provides an energetic reason for the lamellae changing into perpendicular orientation, with the shear thinning. The shear thinning corresponds to the reorientation of the lamellae, while the shear thickening corresponds to the phase transition from lamellar to ribbon, and to cylindrical structure.

1. Introduction

The composites of block copolymers (BCPs) and nanoparticles (NPs) have received great attentions for potential application in nanoscience and nanotechnology.[1–4] Such popularity stems from the ability of BCPs to self-assemble into a variety of periodic mesoscale structures such as spheres, cylinders and lamellae when cooled below a certain temperature (order–disorder transition temperature T_{ODT}).[5,6] The shape and size of such self-assembly structures can be tailored using different compositions, molecular weights, and the interaction parameters between the blocks, respectively. Thus, the microphase separation of BCPs provides a "template" to organize the particles into 3-D ordered arrays within the polymer matrix,[7,8] such as nano-planes, -wires or -spheres, and thereby tailors the properties of the composites. For example, the optical performance and mechanical behavior of the composites are highly sensitive to the specific location of the particles within the polymers.[9] Meanwhile, the particles are not passive and also can alter both the orientation[10] and the morphology[11] of the copolymers microdomains.

In the last decades, many experimental,[9,12–15] theoretical,[16–18] and computer simulation[19–22] studies mainly focused on mixtures of BCPs and spherical NPs. Experimentally, Chiu *et al.* demonstrated that the NPs surface chemistry and size could be used to direct the placement of NPs within BCPs melts. The selective NPs gather at the center of one domain, while the population of the nonselective NPs are centered around the A/B interface.[14] For the small A-coated NPs, the NPs are exclusively located throughout the A domain. For the other extreme of large NPs, they tend to be located at the center of the A domain, where most chain ends lie, in spite of the loss of translational entropy.[9] These experimental observations were affirmed by theoretical predictions of Thompson *et al.*,[18] as well as the computer simulations of Schultz *et al.*[21] To summary, the distribution of NPs within a block copolymer melt is dictated by thermodynamics, namely determined by a complex interplay between entropy and enthalpy within the system.[16] There are enthalpic interactions between the chemically altered NPs and the copolymer blocks. The entropic contribution has two prominent components: the translational entropy of the NPs and the configurational entropy of the polymer chains. Excitingly, this interplay can be tuned by controlling the size, shape and coating of NPs.

Besides spherical structures, NPs also can be produced with a wide range of shapes, including cube, rod, disk and pyramidal.[23] Especially, high aspect-ratio particles, such as nanorods (NRs), will result in polymers nanocomposites processing superior optical and mechanical properties relative to polymers reinforced with an equivalent volume fraction of spherical particles,[24] due to the effect of the additional orientational entropy resulting from the anisotropy of the particles. Recently, there has been considerable interest in studying the self-assembled behaviors of BCPs melts incorporated with anisotropic NRs.[25–31] Experimentally, Zhang *et al.* described the behaviors of CdSe NRs in diblock copolymer templates, PS-*b*-PMMA, one with lamellar nanoscopic channels and the other with cylindrical nanoscopic pores. By choosing the NR dimensions relative to the channel or pore width, they could control the orientation and lateral position of NRs.[25] Béneut *et al.* investigated magnetic NRs confined in a lamellar lyotropic phase. They found that when the NRs are oriented, the texture of the lamellar phase changes accordingly,

[a]*Department of Physics, Zhejiang University, Hangzhou, 310027, P R China. E-mail: lxzhang@zju.edu.cn*
[b]*Department of Physics, Wenzhou University, Wenzhou, 325035, P R China*
[c]*Department of Polymer Science and Engineering, University of Science and Technology of China, Hefei, Anhui, 230026, China*

and interestingly, the lamellar phase induces an attractive interaction between the NRs.[26] In our previous study, we investigated the mixtures of lamellar DBCPs and selective NRs, preferentially attracted by one of the blocks, and found that the loading of NRs induces a series of phase transformations in the polymer microstructure, including lamellar, lamellar/cylindrical mixed, cylindrical and elliptic structures, as well as phase-separated microdomains of DBCPs which in turn affect the NRs spatial distribution and orientation.[31]

Most previous studies on BCPs melts or BCPs/NPs systems are limited to the equilibrium state. However, the complex behavior of these materials away from equilibrium cannot be overstated, given that nonequilibrium conditions are commonly encountered in experiments and manufacturing processes. The shear flow has been regarded as an effective approach to produce long-range order[32] and order–disorder or order–order structural transitions,[33–35] as well as the orientation of self-assembled structures[36–41] for pure BCPs melts. Especially, the lamellar architectures of diblock copolymers (DBCPs) under shear have been well studied.[38–41] Three lamella orientations have been observed: at low shear rates, the parallel (*i.e.*, the lamellar normal is parallel to the velocity gradient direction), the perpendicular (in which the lamellar normal is perpendicular to the velocity gradient direction), and the transverse orientation (that is, the lamellar normal is parallel to the velocity direction). These transitions have been shown to depend on the shear rate (or frequency with oscillatory shear).[41] For the nanocomposites, on the one hand, a number of experimental measurements and simulations have investigated the rheological behavior and morphology of homopolymer/nanoparticle composites under shear.[42–46] For example, Kairn *et al.* demonstrated the shear viscosities, zero-shear viscosities, and the rate of shear thinning all increase with NPs content in both the experimental and simulated systems.[44] One the other hand, there are a few recent studies directly on the dynamic behaviors of block copolymer/nanoparticle composites subjected to shear flow, for spherical NPs.[47–53] Mendoza *et al.* experimentally used the shear to fabricate 3-D ordered arrays of metallic gold NPs embedded in a lamellar structure of a PS-*b*-P4VP diblock.[47,48] Then, they also investigated spherical PS_{327}-*b*-$P4VP_{27}$ block copolymers incorporated with gold NPs. The hybrid block copolymer is able to self-assemble from bcc-spherical to hex-cylindrical morphology. Then the application of the shear flow improves markedly the alignment of these nanocylinders.[49] For the both cases, the gold NPs are incorporated selectively into a specific block of the copolymeric matrix. Kalra *et al.* performed molecular dynamics (MD) simulations to model the behaviors of symmetric diblock copolymer/nanoparticle systems subjected to shear or elongational flow. They summarized that the external field, especially for shear flow, could be as a beneficial mean to control the three-dimensional arrangement of spherical NPs within diblock copolymers, and the presence of NPs significantly influences the shear-induced transitions in lamellae orientation.[50,51] However, studies about the hybrid systems of block copolymers and anisotropic NRs under shear are comparatively few, whether experiments or theories and simulations.

In the current work, we extend the dissipative particle dynamics (DPD) method to investigate the behaviors of symmetric diblock copolymer/nanorod composites subjected to steady shear flow. We take the cases of both selective and nonselective NRs with a fixed NR length over a range of shear rates. Based on the anisotropy of NRs relative to classical spherical NPs, we aim to answer two questions from simulations. (1) How does the shear flow direct the orientation of DBCPs microstructure, and the phase behaviors of NRs (including the spatial distribution and orientation)? (2) In turn, how does the presence of anisotropic NRs affect the shear-induced orientation and morphology transition in DBCPs self-assembly?

2. Model and simulation method

The dissipative particle dynamics (DPD) method[54] is referred as a new simulation technique, appropriate for the investigation of the generic properties of macromolecular systems. Within the DPD, fluid particles are coarse grained into 'beads' or DPD particles. The total force acting on a particular bead i is the sum of a conservative force, a dissipative force and a random force

$$\vec{f}_i = \sum_{i \neq j} \left(\vec{F}_{ij}^{\mathrm{C}} + \vec{F}_{ij}^{\mathrm{D}} + \vec{F}_{ij}^{\mathrm{R}} \right) \tag{1}$$

$$\vec{F}_{ij}^{\mathrm{C}} = a_{ij}\omega(r_{ij})\hat{r}_{ij} \tag{2}$$

$$\vec{F}_{ij}^{\mathrm{D}} = -\gamma\omega^2(r_{ij})(\hat{r}_{ij}\cdot\vec{v}_{ij})\hat{r}_{ij} \tag{3}$$

$$\vec{F}_{ij}^{\mathrm{R}} = \sigma\omega(r_{ij})\theta_{ij}\hat{r}_{ij} \tag{4}$$

The conservative force $\vec{F}_{ij}^{\mathrm{C}}$ is the soft repulsion acting along the intermolecular vector, where a_{ij} is a maximum repulsion between beads i and j; and $\vec{r}_{ij} = \vec{r}_i - \vec{r}_j$, $r_{ij} = |\vec{r}_{ij}|$, $\hat{r}_{ij} = \vec{r}_{ij}/r_{ij}$. For the weight function $\omega(r)$, we adopt the commonly used form:

$$\omega(r) = \begin{cases} 1 - r/r_{\mathrm{c}} & r_{ij} < r_{\mathrm{c}} \\ 0 & r_{ij} \geq r_{\mathrm{c}} \end{cases} \tag{5}$$

which is a r-dependent weight function vanishing for $r_{ij} \geq r_{\mathrm{c}}$, where r_{c} is the cutoff radius. The other two forces ($\vec{F}_{ij}^{\mathrm{D}}$and $\vec{F}_{ij}^{\mathrm{R}}$) act as a heat source, which effectively combine to thermostat the system. $\vec{v}_{ij} = \vec{v}_i - \vec{v}_j$ and θ_{ij} is a randomly fluctuating variable with Gaussian statistics: $\langle\theta_{ij}(t)\rangle = 0$ and $\langle\theta_{ij}(t)\theta_{kl}(t')\rangle = (\Delta_{ik}\Delta_{jl} + \Delta_{il}\Delta_{jk})\Delta(t - t')$. Also, there is a relation between the friction coefficient γ and the noise amplitude σ as follows:

$$\sigma^2 = 2\gamma k_{\mathrm{B}}T \tag{6}$$

where k_{B} is Boltzmann's constant and T is the temperature. Referring to the classical DPD studies by Groot,[55] in our simulation we set $\gamma = 6.57$ with $\sigma = 3.62$ according to eqn (6). In DPD, it is convenient to use reduced units. The unit of length is defined by the cutoff radius r_{c}, the unit of mass is defined by the particle mass m (which is chosen to be the same for all the particles), and the unit of energy is defined by $k_{\mathrm{B}}T$.[55] Additionally, for the polymers, the spring force $\vec{f}_i^{\mathrm{S}}$, which acts between the connected beads in a chain, has the form of

$$\vec{f}_i = \sum_j C\,\vec{r}_{ij} \tag{7}$$

where C is a harmonic type spring constant for the connecting pairs of beads in a polymer chain, chosen to be equal to 4.0 here.[55]

For the rigid nanorod, according to the approach taken by previous studies[31,56–58] in the DPD simulation, it can be constructed by a number of DPD beads N_r arranged in a straight line, with a fixed small distance D_{b-b} between consecutive beads. Naturally, the length of a rod can be calculated equivalently by $L_r = (N_r - 1)D_{b-b}$. In order to avoid undesired penetration of fluid particles into the NRs, and overlap between NRs, the number density of the DPD particles in a nanorod is larger than that of the fluids (or DBCPs). Here, we set $D_{b-b} = 0.3$ with a fixed $N_r = 6$, so the NR length L_r equals to 1.5 according to the definition.[31,58] Here, the ratio range of L_r/L_0 (NR length/period width of DBCPs) is about 0.33,[31] comparable to the experimental ratio range of L_r/L_0 = 10–60 nm/60 nm = 0.17–1.0.[25,59,60] Moreover, for the NRs, a constraining routine is used to keep the inner particles aligned and equidistant during the simulation. In short, the forces on the DPD particles of a NR are converted into a net force on the two end DPD particles, and the equations of motion for these two DPD particles are solved, using the standard shake routine to keep them at a fixed distance. The positions of the $N_p - 2$ intermediate DPD particles are then readily calculated by a linear interpolation at the end of each time-step.[56] The Newton equations for all particles' positions and velocities are integrated by a modified version of the velocity Verlet algorithm with the step size of $\Delta t = 0.04\tau$, where τ is the natural unit of time defined as $r_c\sqrt{m/k_BT}$.[61]

Here, we consider the symmetric DBCPs melts (A_5B_5) incorporated with two types of NRs (selective/nonselective). The number density of the fluid system is $\rho = 5$, and then the repulsion parameter a_{ij} in eqn (2) is related to the Flory–Huggins χ-parameter by:

$$a_{ii}\rho = 75k_BT \tag{8}$$

$$a_{ij} \approx a_{ii} + 1.45\chi_{ij}\ (\rho = 5) \tag{9}$$

where the repulsion parameter between particles of the same type $a_{ii} = 15k_BT$ to correctly describe the compressibility of the water.[61] Correspondingly, the values of a_{ij} between the three types of DPD beads (represented by A, B and N), are given by $a_{AA} = a_{BB} = 15$, and $a_{AB} = a_{NN} = 30$. At the same time, a_{AN} and a_{BN} change according to the surface chemistry of NRs. Here, the A-selective NRs corresponds to $a_{AN} = 15$ and $a_{BN} = 30$, while the nonselective NRs corresponds to $a_{AN} = 15$ and $a_{BN} = 15$, where the NRs concentration for both types are represented by ϕ_A and ϕ_N, respectively.

To impose steady shear, we use SLLOD equations of motion:[62]

$$\dot{\vec{r}} = \vec{p}_i/m + \hat{i}\,\dot{\gamma}y_i \tag{10}$$

$$\dot{\vec{p}} = \vec{F} - \hat{i}\,\dot{\gamma}p_{yi} \tag{11}$$

where $\vec{p}_i$ is the momentum of particle i, $\dot{\gamma}$ is the shear rate and $\hat{i}$ is the unit vector in the x-axis direction. The flow direction is parallel to the x-axis direction, the y-axis refers to the velocity gradient, and the z-axis represents the transverse direction. Meanwhile, we employ the Lees–Edwards periodic boundary condition to maintain the steady and linear velocity gradient,[62,63] wherein two opposing periodic images are incrementally moved in opposite directions consistent with the applied shear rate. One of the most important parameters which characterizes rheological properties is the shear viscosity, directly relative to the pressure tensor P, which is measured by:[62,63]

$$P_{\alpha\beta} = \frac{1}{V}\left\langle \sum_i \frac{p_{i,\alpha}p_{i,\beta}}{m_i} \right\rangle + \frac{1}{V}\left\langle \sum_i \sum_{j>i} F^C_{ij,\alpha}r_{ij,\beta} \right\rangle \tag{12}$$

where α, β are the Cartesian indices. Shear viscosity in association with the only nonvanishing off diagonal component

$$P_{xy} = -P_{yx} \text{ is given by: } \eta = -P_{xy}/\dot{\gamma} \tag{13}$$

where η is the non-Newtonian shear viscosity.

The simulations are performed in a cubic box of constant volume $V = 11 \times 11 \times 11$, with periodic boundary conditions applied in all three directions. The simulated systems contain about $N_p = 6655$ DPD polymer particles for the density of $\rho = 5$, and $\varphi/(1 - \varphi) \times N_p$ DPD rod particles, where φ represents the NRs concentration. Our A_5B_5 DPD diblock copolymer model can be considered to mimic low molecular weight diblock copolymers such as polyisoprene-polystyrene (PI-PS, approximately 8000 g mol^{-1}) with a volume fraction of PI approximately 0.5.[64] According to a coarse-graining procedure given by Maiti *et al.*,[65] the cutoff radius r_c is approximately 20 Å according to $r_c = (\rho V_b)^{1/3}$, where V_b is the volume of one DPD particle, so the box length corresponding to $L = 11$ is approximately 220 Å. Meanwhile, the dimensionless shear rate is $\dot{\gamma} \propto (3k_BT/m)^{1/2}$, reduced by a characteristic length, obviously, taking $1/s$ as the unit.[41] The maximum value of shear rate used here is $\dot{\gamma} = 0.21$ in the reduced unit, which is not too large and can avoid the potential microturbulence, and even distortion. Moreover, we start the simulations in which the lamellae of nanocomposites are initially oriented transverse to the shear direction (*i.e.*, the lamellar normal is parallel to the velocity direction), and evolve the system at least 150000 timesteps until a final stable state is achieved. To eradicate the finite-size effect, some extra simulations have been carried out by enlarging the box size to $V = 13 \times 13 \times 13$ (N_p = 10985), also by starting from the transverse quiescent state. After much longer simulation times, similar results are found, which will be discussed in the following section in more detail.

3. Results and discussion

In our previous work,[31] we examined the lamellar DBCPs/NRs mixtures under equilibrium state (*i.e.* no shear flow). As varying the concentration of NRs with a fixed NR length, for the selective NRs case, it could induce rich phase transitions from lamellar to lamellar/cylindrical mixed to cylindrical, even to elliptic structures; for the nonselective NRs case, there is no order–order but order–disorder transition, due to a reduction in segregation between blocks A and B. To readily compare our new finding with the previous work, in the current study the initial states all correspond to the previous obtained phase diagrams.[31] To preserve lamellar morphology in the nanocomposites, we keep the NRs concentration below 15%, which is further divided into two cases: (1) the low concentration with $\phi_{A(N)} = 5\%$; (2) the high

concentration with $\phi_{A(N)} = 10$ or 15%. Both selective and nonselective NRs are considered throughout our simulations.

3.1 The low NRs concentration

We conduct simulations for a pure DBCP melt system under different shear rates ranging from $\dot{\gamma} = 0$ to 0.15, and find that the transverse lamellar phase is stable when $\dot{\gamma} < 0.01$. For $0.01 \leq \dot{\gamma} < 0.05$, the transverse lamellar phase transforms into a parallel lamellar phase, whereas for $\dot{\gamma} \geq 0.05$, the transverse lamellar phase reorients into a perpendicular lamellar phase. The typical snapshots of DBCPs with $\dot{\gamma} = 0$, 0.01 and 0.09 are shown in Fig. 1a–c, corresponding to the transverse, parallel and perpendicular lamellar phases, respectively. Especially for perpendicular lamellar phase, we plot the density profile of blocks A and B along the z-axis direction in (d), indicating strongly segregated blocks with ordered lamellae, consistent with the snapshot shown in (c). The observations demonstrate the lamellar phase preferentially adopts the parallel orientation at low shear rates and the perpendicular orientation at high shear rates, which is in agreement with previous studies by Koppi *et al.* in experiments.[66] Fraser *et al.* used MD simulations to study how shear flow affected the orientation of lamellar structures, and our results are in accord with their simulations. They observed that the perpendicular phase has lower internal energy and smaller entropy production than the parallel phase, and is more stable at relatively high shear rates.[40]

Then, we investigated the symmetric diblock copolymers mixed with A-selective NRs, in which the NRs concentration is $\varphi_A = 5\%$. The simulation snapshots of systems with $\dot{\gamma} = 0$, 0.01 and 0.08 are presented in Fig. 2(a1)–(c1), showing transverse, parallel and perpendicular lamellar morphologies, respectively. Similar to pure DBCPs under shear, an excellent agreement with experimental observations is found; that is, at low shear rate, the lamellar phase preferentially aligns parallel to the shear direction, and at high shear rate, the lamellar phase preferentially aligns perpendicular to the shear direction.[66] However, the transverse-to-perpendicular transition takes place at a higher shear rate, $\dot{\gamma} = 0.08$, than that of the pure DBCPs at $\dot{\gamma} = 0.05$. In these lamellar phases, the NRs are exclusively distributed within the A phase domain, due to the preferentially attractive interaction between NRs and blocks A.[31] For the perpendicular lamellae shown in Fig. 2(c1), the density profile of A, B blocks, and NRs along the z-axis direction, is plotted in Fig. 2(d1). The A-selective NRs density curve in yellow exhibits a maxima at the center of the preferred A domain, while the NRs concentration in the B domain remains zero in spite of the shear. The results are qualitatively similar to the previous studies for DBCPs and spherical NPs mixtures under equilibrium condition, which shows the NPs tend to be located at the center of the preferred domain, where most chain ends lie, to decrease the conformational entropy of the polymer chains.[9,13,21] To verify that our DPD results are not affected by the box size, we performed additional DPD simulations for the larger system, $V = 13 \times 13 \times 13$, with the same shear rates $\dot{\gamma}$, and the results are in good agreement with those for the smaller system, $V = 11 \times 11 \times 11$, which are shown in Fig. 2(a2)–(d2).

For comparison, we also consider the symmetric DBCPs mixed with nonselective NRs, where the concentration is $\varphi_N = 5\%$. Again, we find that the reorientation of lamellae is from ordered transverse to parallel, and then perpendicular lamellae as the shear rate increases. In Fig. 3, we display simulation snapshots of systems with $\dot{\gamma} = 0$, 0.01 and 0.03, showing transverse, parallel and perpendicular lamellar structures, respectively. Though the shear-induced orientation transitions are consistent with pure DBCPs and A-selective NRs cases, this time transverse-to-perpendicular transition takes place at lower shear rate, $\dot{\gamma} = 0.03$, than the pure DBCPs case of $\dot{\gamma} = 0.05$. The density profile for perpendicular lamellar structure shown in Fig. 3(c), is plotted in Fig. 3(d), indicating the NRs are basically centered around the A/B interface, while the NRs concentrations are not zero in A and B domains due to the equal favorable interactions between NRs and A (and B) domains. This reveals that the enthalpic effects from the interactions between nonselective NRs and blocks A (and B) overcome the entropic effects from the conformation transition of copolymer chains. In other words,

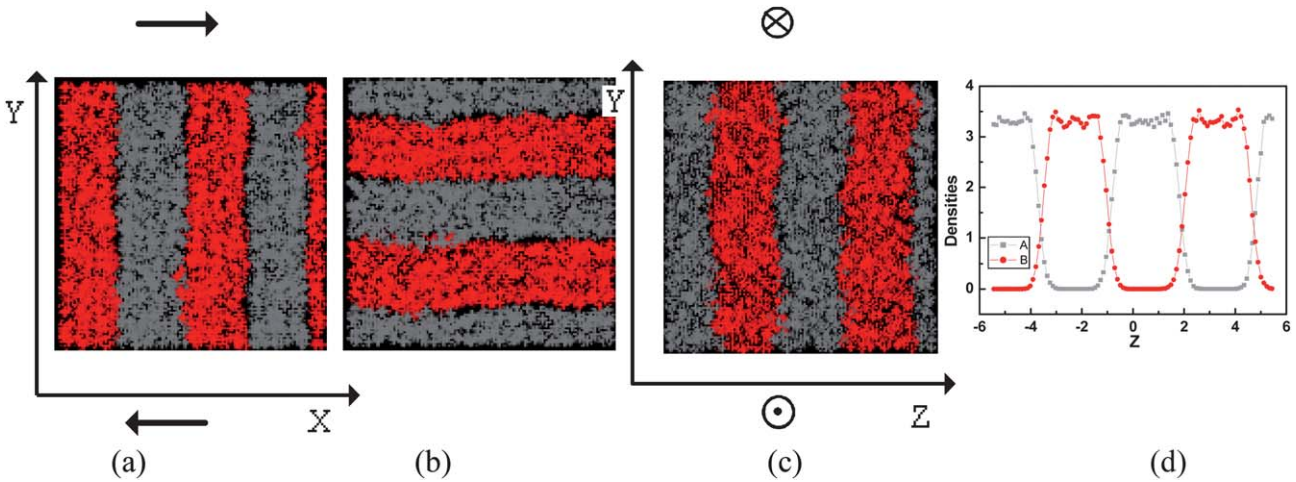

Fig. 1 Pure symmetric DBCPs under shear: (a–c) snapshots with the shear rates of $\dot{\gamma} = 0$, 0.01, 0.05 and (d) density profile for $\dot{\gamma} = 0.05$ corresponding to (c). A and B blocks are presented in gray and red, respectively. The arrows show the imposed shear direction, parallel to the x-axis. The view in (a) and (b) is perpendicular to the shear direction (*i.e.*, along the z-axis), while the view in (c) is parallel to the shear direction (*i.e.*, along the x-axis).

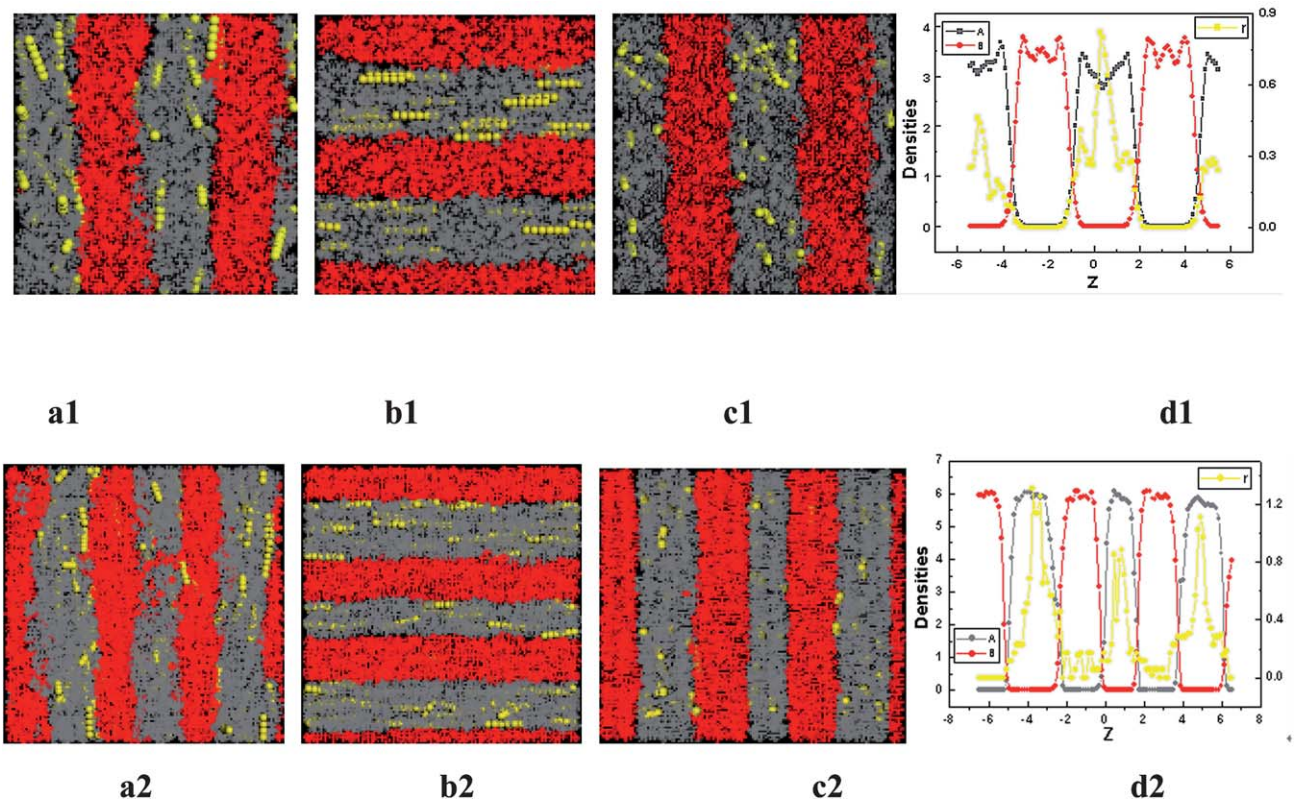

Fig. 2 Symmetric DBCPs mixed with A-selective NRs under shear: (a1)–(c1) snapshots with the shear rates of $\dot{\gamma} = 0$, 0.01, 0.08, and (d1) density profile for $\dot{\gamma} = 0.08$ corresponding to (c1). The corresponding simulations for 13 × 13 × 13 DPD units systems are also shown in (a2)–(d2). Here NRs are presented in yellow and the NRs concentration is $\varphi_A = 5\%$. The view in (a1), (b1) and (a2), (b2) is perpendicular to the shear direction, while the view in (c1) and (c2) is parallel to the shear direction.

despite the block copolymers being incorporated with anisotropic NRs under the shear flow, the interplay between entropy and enthalpy involving blocks A, B, and surface chemistry of NRs, still remains dominant for directing the equilibrium location of NRs within polymer matrix.

For the above three systems shown in Fig. 1–3, although there are similar reorientation transitions of lamellae: transverse-to-parallel, and transverse-to-perpendicular, the latter transitions take place at three different shear rates for the three systems: $\dot{\gamma} = 0.05$ for pure DBCPs, $\dot{\gamma} = 0.08$ for A-selective NRs/DBCPs system, and $\dot{\gamma} = 0.03$ for nonselective NRs/DBCPs system, respectively. Rheological measurements can be performed to resolve the structure of a self-assembled copolymer/nanorod system. Both Koppi *et al.*[66] in experiment and Guo[67] by MD simulation had shown that the shear viscosity relates to the orientation of the LAM phase, *i.e.*, $\eta_{perpendicular} < \eta_{parallel}$. A sharp decrease in shear viscosity is seen at the critical shear rate $\dot{\gamma}_c$, where a transition from initial alignment to perpendicular orientation takes place.[67,68] The calculated shear viscosity η as a function of the shear rate $\dot{\gamma}$ for the three systems is shown in

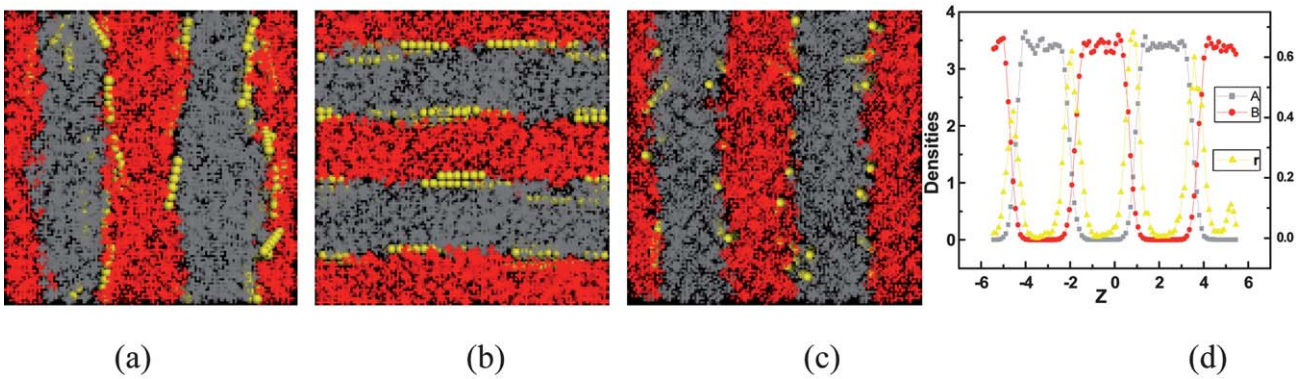

Fig. 3 Symmetric DBCPs mixed with nonselective NRs under shear ($\varphi_N = 5\%$): (a)–(c) snapshots with the shear rates of $\dot{\gamma} = 0$, 0.01, 0.03, and (d) density profile for $\dot{\gamma} = 0.03$ corresponding to (c). The views in (a) and (b) are perpendicular to the shear direction, while the view in (c) is parallel to the shear direction.

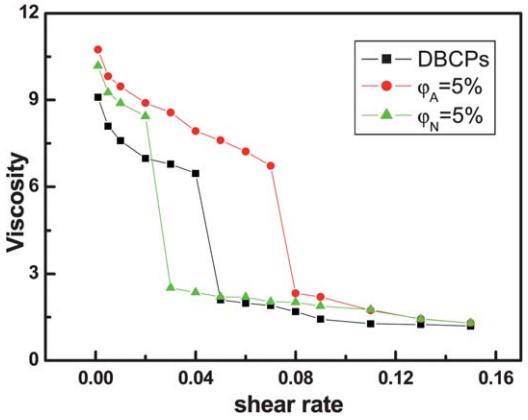

Fig. 4 The shear viscosity η as a function of the shear rate $\dot{\gamma}$ for pure DBCPs, A-selective NRs/DBCPs ($\varphi_A = 5\%$) and nonselective NRs/DBCPs ($\varphi_N = 5\%$).

Fig. 4. Take the pure DBCPs (plotted in black) case for example. First, corresponding to the small shear rates with $\gamma < 0.05$, the shear viscosity η gradually decreases following a transverse-to-parallel transition. After that, the shear viscosity sharply drops at a shear rate of 0.05, indicating an orientation flip to perpendicular morphology,[67,68] also seen from the snapshot in Fig. 1(c). The plots (in red and green) for nanocomposite systems show a shift of critical shear rate to a higher value $\dot{\gamma}_c = 0.08$ for A-selective NRs/DBCPs systems, and a lower value $\dot{\gamma}_c = 0.03$ for the nonselective NRs/DBCPs case, as compared to a neat DBCPs. Finally, the shear viscosity decreases smoothly with increasing shear rate in the region of perpendicular lamellae. In our simulations, $\eta_{perpendicular}$ is smaller than $\eta_{parallel}$, which is in agreement with the experimental and simulation results that the shear viscosity relates to the orientation of the lamellar phase.[66–68] As the shear viscosity shown in Fig. 4, for the above three systems, the critical shear rates $\dot{\gamma}_c$ of transverse-to-perpendicular transition are well consistent with the results from snapshots in Fig. 1–3. In other words, the presence of selective/nonselective NRs delays or advances the shear-induced transition from transverse to perpendicular lamellae. Essentially, for the A-selective NRs case, the NRs helps to strengthen the cohesive forces within A domain by polymer bridging, thereby increasing the segregation $(\chi_N)_{eff}$ between A and B blocks. The increase of A/B incompatibility will lead to increasing the order–disorder transition temperature (T_{ODT}), making the order–order transition more difficult, and therefore increasing the critical shear rate $\dot{\gamma}_c$. The effect of transition temperature T_{ODT} on the critical shear rate $\dot{\gamma}_c$ has been well studied.[69] Meanwhile, Guo *et al.* summarized that the critical shear rate increases as the segregation between two blocks increases.[67] For nonselective NRs case, NRs preferentially located at the A/B interface, help to decrease the interfacial tension by reducing the number of A/B contacts, thereby weakening the segregation $(\chi_N)_{eff}$ between blocks A and B. By a similar analysis as for the A-selective NRs case, conversely, a decrease in A/B incompatibility will lead to decreasing the critical shear rate. Additionally, the NRs orientation is highly sensitive to the directional fields, such as shear or electric field, and therefore, NRs are oriented immediately to the shear direction, due to the effect of the additional orientational entropy.

3.2 The high NRs concentration

Here, we mainly consider the case in which DBCPs melts are incorporated with a relatively high concentration of A-selective NRs. The imposed shear rate ranges from $\dot{\gamma} = 0$ to 0.21 at intervals of 0.005/0.01 at lower rate and intervals of 0.02 at higher rate. Fig. 5 shows simulation snapshots of nanocomposites with $\phi_A = 15\%$ under shear rates of $\dot{\gamma} = 0$, 0.01, 0.03, 0.05, 0.06, 0.09, 0.13 and 0.21, corresponding to transverse lamellar, parallel lamellar, diagonal lamellar, ribbon, cylindrical, ribbon, diagonal lamellar, and perpendicular lamellar structures, respectively, where the NRs are expelled into the A domain. In Fig. 5(a), the initial lamellar structure is also transverse to shear direction. From Fig. 5, we can see that the common shear-induced reorientations of transverse-to-parallel at low rates from $\dot{\gamma} = 0.001$ to 0.02 in Fig. 5(b), and transverse-to-perpendicular at high rates from $\dot{\gamma} = 0.15$ to 0.21 in Fig. 5(h). A transverse-to-diagonal reorientation of lamellae appears at $\dot{\gamma} = 0.03$ and 0.13 in Fig. 5(c) and (g). The diagonal lamellae (*i.e.*, with the lamellae oriented in the shear direction but diagonally between a parallel and perpendicular alignment) can be seen as a transient phase between parallel and perpendicular lamellae.[40,41] As already discussed by Lísal *et al.*, values of the potential energy and entropy production for the diagonal lamellar phases lie between the corresponding values for the parallel and perpendicular lamellar phases.[41] Interestingly, besides the reorientations in lamellae, the shear-induced morphology transitions of lamellae-to-ribbon and lamellae-to-cylinder take place at intermediate rates from $\dot{\gamma} = 0.05$ to 0.09 in Fig. 5(d)–(f). The ribbon structure has been observed in previous study,[31] which also can be taken as a transient phase structure between lamellar and cylindrical morphologies. In the case of $\dot{\gamma} = 0.06$ in Fig. 5(e), the cylinders are stable and do not vanish while keeping on shearing. Compared to the pure DBCPs or DBCPs/NRs with $\varphi_A = 5\%$, the shear induces not only the reorientations of lamellae to shear direction, and but also a series of morphology transformations for DBCPs/NRs nanocomposites. The latter is contributed to the presence of selective NRs with a relatively high concentration. Interestingly, Fig. 5 reveals that the shear-induced phases experience a symmetrical and reversible process: from lamellar to ribbon to cylindrical phase with varying from $\dot{\gamma} = 0.01$ to 0.06 shown in Fig. 5(b)–(e), and then conversely, from cylindrical to ribbon to lamellar structure with varying from $\dot{\gamma} = 0.06$ to 0.21 shown in Fig. 5(e)–(h). These results are similar to the symmetric phase transitions caused by varying the block composition f according to the morphology diagram of diblock copolymer melts,[70] suggesting that the presence of a certain concentration range of A-selective NRs under shear may affect the effective block composition (f_{eff}) in composites, and therefore causes the phase transitions between lamellae and cylinder, which will be illustrated by the properties of copolymers and NRs on the molecule level, respectively.

Fig. 6(a) shows the shear viscosity of copolymers as a function of shear rate, which can be roughly divided into three regions, corresponding to the snapshots shown in Fig. 5. The first region corresponds to the low rates with $\dot{\gamma} < 0.05$, where the shear viscosity decreases dramatically with increasing shear rate, followed by the two reorientations of transverse-to-parallel and transverse-to-diagonal shown in Fig. 5(b) and (c). Then, the

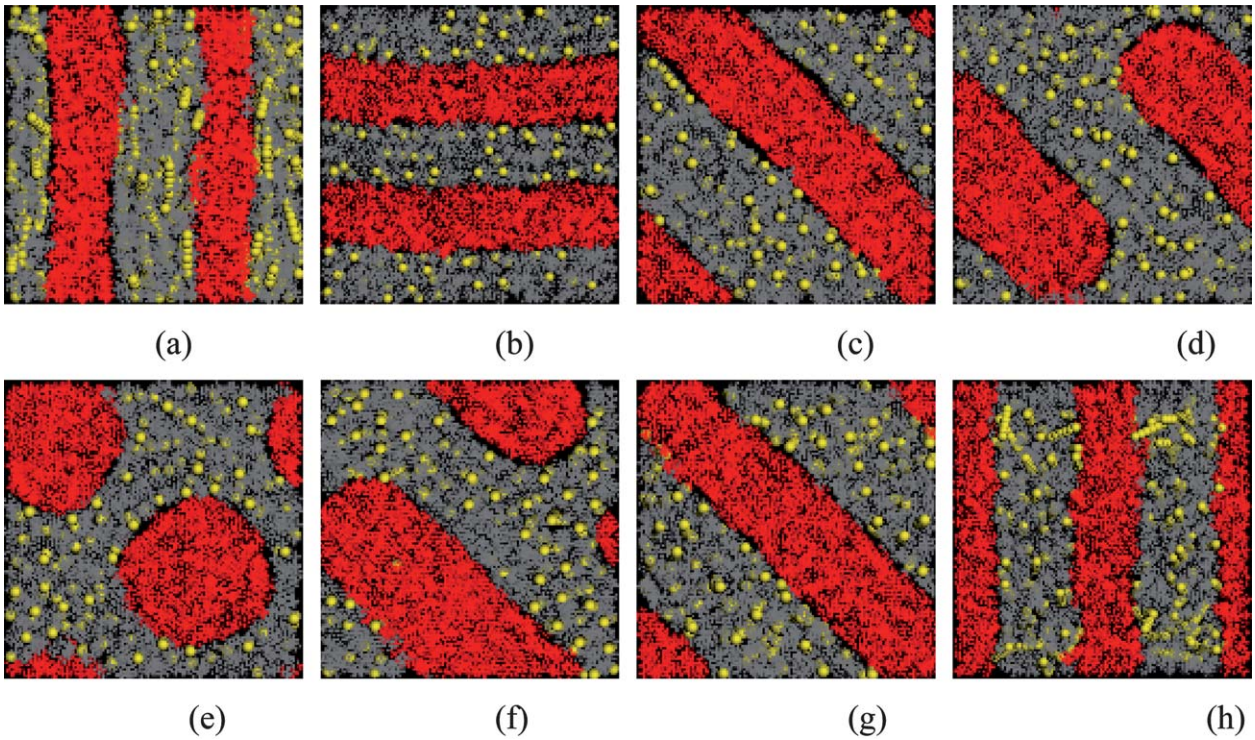

Fig. 5 Snapshots of symmetric DBCPs mixed with A-selective NRs ($\varphi_A = 15\%$) at $\dot{\gamma} = 0$, 0.01, 0.03, 0.05, 0.06, 0.09, 0.13 and 0.21 in (a)–(h). The view of the initial lamellar structure in (a) is perpendicular to the shear direction, while the view in (b)–(h) is parallel to the shear direction.

shear viscosity first increases and decreases again from $\dot{\gamma} = 0.05$ to 0.12 and shows local convexes. Corresponding to Fig. 5(d)–(f), in this region no reorientations in lamellae are induced, and the morphology transitions of lamellar-to-ribbon and lamellar-to-cylindrical structures are observed. After that, the shear viscosity decreases gradually with shear rate in the third region from $\dot{\gamma} =$ 0.13 to 0.21, where the diagonal lamellae is found again, and finally the perpendicular lamellar phase is obtained, corresponding to Fig. 5(g) and (h). Generally, the shear viscosity decreases with shear rate increases, corresponding to shear thinning, in which the layer width is slightly decreased so that transverse lamellae can adopt parallel or perpendicular orientations.[41] However, the local convexes in viscosity corresponds to the shear-induced thickening, where the lamellar is transformed into ribbon and cylindrical phase, whose width/diameter is larger than the width of the layer.

Fig. 6(b) shows the mean-squared end-to-end distance of copolymer chains $\langle R^2_{end} \rangle$ in x-, y- and z- directions as a function of shear rate $\dot{\gamma}$, which also corresponds and manifests the reorientations and morphology transitions shown in Fig. 5. In Fig. 6(b), $\langle R^2_x \rangle$ grows steadily with shear rate, suggesting that the shear tilts and stretches each chain, *i.e.*, an orientation of chains along the flow direction, which promotes shear-induced thinning. At the low rates from $\dot{\gamma} = 0.001$ to 0.02, $\langle R^2_y \rangle > \langle R^2_z \rangle$ confirms that the lamellae adopt parallel orientation. At the high rates from $\dot{\gamma} = 0.15$ to 0.21, a discontinuous jump of $\langle R^2_z \rangle$ and a sharp drop of $\langle R^2_y \rangle$ take place at $\dot{\gamma} = 0.15$, indicating the orientation transition from transverse to perpendicular. For

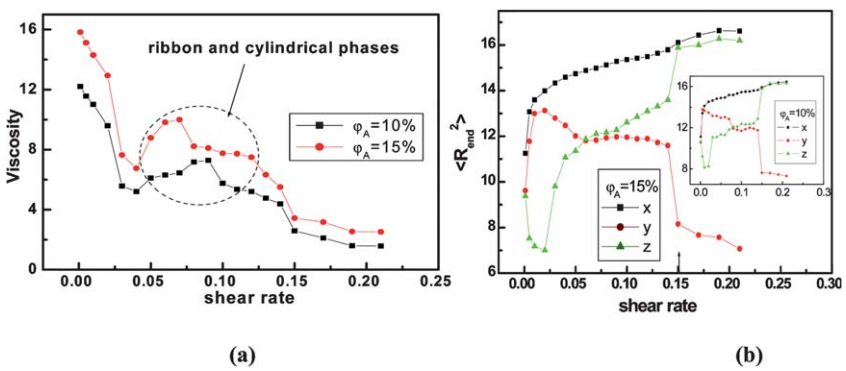

Fig. 6 (a) The shear viscosity η as a function of shear rate $\dot{\gamma}$. (b) Mean-squared end-to-end distance of copolymer chains in the x-, y- and z-direction as a function of shear rate $\dot{\gamma}$ for $\varphi_A = 15\%$; the inset corresponds to the case of $\varphi_A = 10\%$.

$\dot{\gamma} > 0.15$, $\langle R_y^2 \rangle < \langle R_z^2 \rangle$ is observed in the shear-induced perpendicular lamellae. At the intermediate case from $\dot{\gamma} = 0.03$ to 0.14, $\langle R_y^2 \rangle$ decreases gradually with shear rate, while $\langle R_z^2 \rangle$ increases gradually, corresponding to the regions of shear-induced reversible morphology transitions mentioned above: from diagonal lamellar to ribbon to cylindrical phase with varying from $\dot{\gamma} = 0.03$ to 0.06 in Fig. 5(c)–(e), and conversely, from cylindrical to ribbon and return to diagonal lamellar structure with varying from $\dot{\gamma} = 0.06$ to 0.14 in Fig. 5(e)–(g). During this region, $\langle R_y^2 \rangle \approx \langle R_z^2 \rangle$ indicates the isotropy of shear-induced microphase structure in the yz-plane, marking the cylindrical phase formed, obviously at $\dot{\gamma} = 0.06$ and 0.07. The case of $\varphi_A = 10\%$ is also considered in Fig. 6(a) and (b), whose results is similar to $\varphi_A = 15\%$ case.

In the following we turn to monitor the dynamic properties of NRs in the diblock matrix, such as the spatial orientation and distribution. The spatial orientation of NRs can be measured quantitatively as follow:

$$\langle P(\cos\theta) \rangle = \langle (3\cos^2\theta - 1)/2 \rangle \quad (14)$$

Where θ is the angle of NR orientation with respect to the shear direction (*i.e.*, x-axis direction). The average NRs orientation $\langle P(\cos\theta) \rangle$ will take values of -0.5, 0 and 1 for rods that are perpendicular, randomly oriented and parallel to the x-axis.[31] Fig. 7(a) shows the average NRs orientation $\langle P(\cos\theta) \rangle$ as a function of shear rate. For shear rates of $\dot{\gamma} < 0.13$, the value of $\langle P(\cos\theta) \rangle$ remains nearly constant at 1.0, indicating NRs are well oriented to shear direction. When the shear rate is increased up to 0.13 or even higher, the value of $\langle P(\cos\theta) \rangle$ first drops dramatically and then decreases little with shear rate increases. As expected, the NRs should be well oriented to the shear flow direction, while here the NRs orientation $\langle P(\cos\theta) \rangle$ decreases a little at high shear rates, caused by the disturbance from copolymer chains. As shown by $\langle R_{end}^2 \rangle$ in Fig. 6(b), with increasing shear rate, the chains will be tilted and stretched. The stretched chains will energetically constraint the NRs behavior freedom, leading to a decrease in $\langle P(\cos\theta) \rangle$. The curve for $\varphi_A = 10\%$ case shows the same trend to $\varphi_A = 15\%$ in Fig. 7(a).

The spatial distribution of NRs within copolymer matrix can be measured by the pair correlation function $g(r)$ defined as[71]

$$g(r) = \frac{V}{N^2} \left\langle \sum_i \sum_j \delta(r - r_{ij}) \right\rangle \quad (15)$$

where N is the number of NRs, and $\delta(r)$ is the Dirac delta function. In this work, for the NRs well oriented to shear direction, we calculate the correlation function $g(r_{yz})$ by counting the head-particle position of each NR projected in $_{yz}$-plane. According to the NRs orientation shown in Fig. 7(a), the pair correlation function $g(r_{yz})$ for different shear rates $\dot{\gamma} = 0.01$, 0.03 and 0.06 are shown in Fig. 7(b), corresponding to the parallel lamellar, diagonal lamellar and cylindrical structures, respectively. The right shift of peaks in $g(r_{yz})$ curves suggests the NRs become more and more dispersed. Moreover, within the three phase structures (parallel and diagonal lamellae and cylinder), the corresponding average distances inter-NRs d_r are calculated as $d_r = 2.26$, 2.43, and 2.55, respectively, which also indicates the NRs immersed in the cylindrical phase are more dispersed than that in lamellar phase. As expected, the NRs subjected to shear flow, trend to disperse within the preferential A domain. In addition to this, the pair correlation functions $g(r_{yz})$ for NRs/homopolymer (A_{10}) nanocomposites under shear rates of $\dot{\gamma} = 0.01$, 0.06 and 0.09 are also plotted in the inset of Fig. 7(b), which also indicates the dispersion of NRs is improved first by increasing the imposed shear rate, and consequently the dispersion is stabilized under a high shear rate or even higher, in agreement with the simulations on the NPs dispersion in shear-flow polymer fluids.[46]

Combining Fig. 6 with Fig. 7, we can see that the phase behaviors of copolymer chains and NRs under shear flow are co-responsible for the final morphology of nanocomposites. The schematic process shown in Fig. 8 offers a clear view about the interplay between DBCPs and NRs under shear. For the pure DBCPs case shown in the upper part of Fig. 8, as the shear rate increases, the transverse lamellae is oriented into a parallel alignment at low shear rates, and then reoriented into a perpendicular alignment at the critical shear rate ($\dot{\gamma}_c = 0.05$). Fraser *et al.* found that the perpendicular lamellae always associated with a lower potential energy, thus providing an energetic reason favoring such transition from transverse to perpendicular arrangement at higher shear rates.[40] Moreover, due to the shear thinning, the energetically favored perpendicular lamellar structures have a reduction in lamellar spacing d_p at shear rates

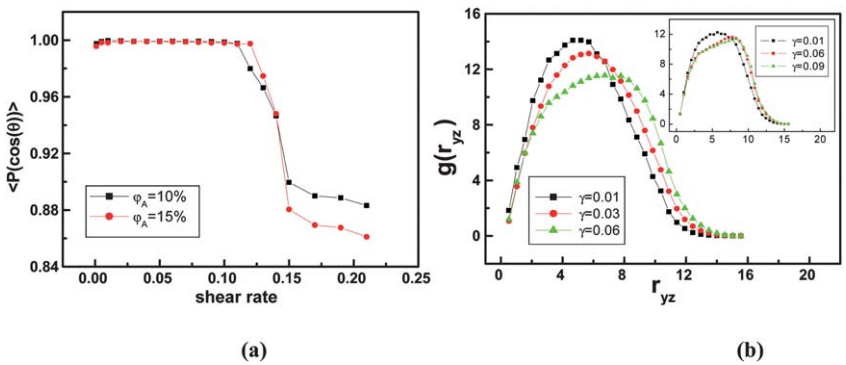

Fig. 7 (a) Average NRs orientation $\langle P(\cos\theta) \rangle$ as a function of shear rate $\dot{\gamma}$. (b) The pair correlation function $g(r_{yz})$ as a function of the distance r_{yz} between NRs for $\varphi_A = 15\%$ at $\dot{\gamma} = 0.01$, 0.03 and 0.06, corresponding to the parallel lamellar, diagonal lamellar and cylindrical phase, respectively. The inset corresponds to the homopolymers (A_{10}) mixed with A-selective NRs ($\varphi_A = 15\%$) at $\dot{\gamma} = 0.01$, 0.06 and 0.09.

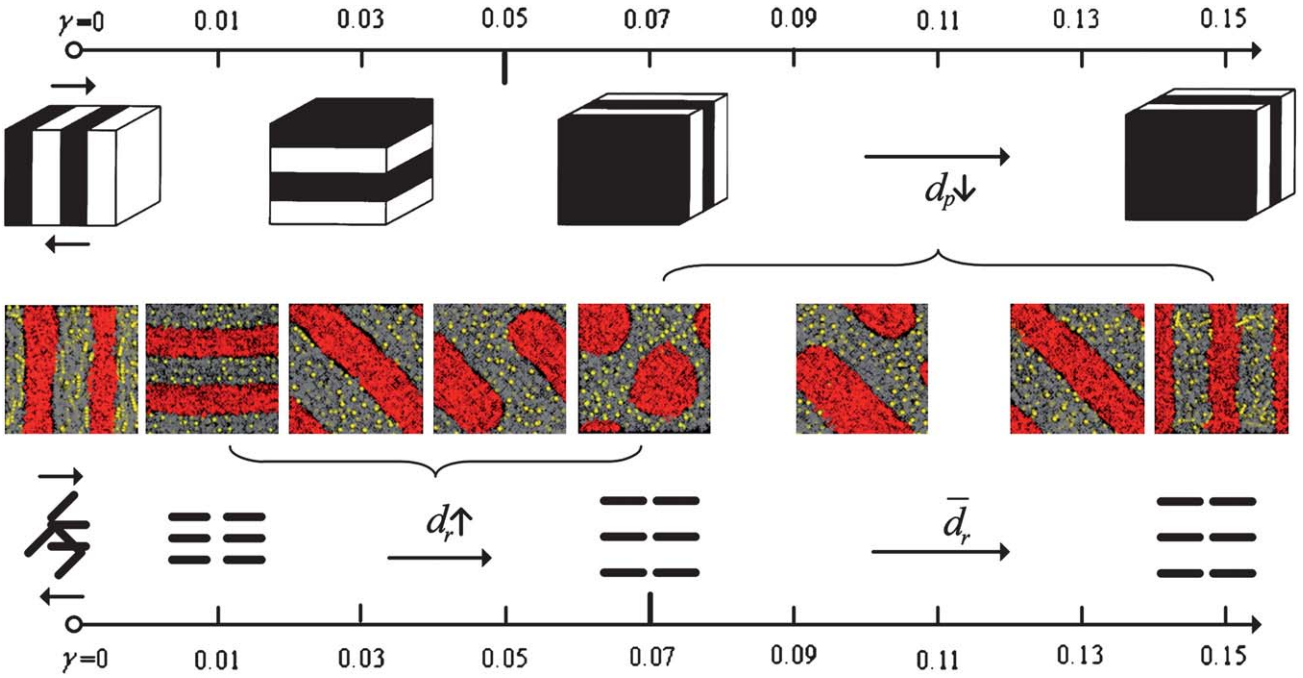

Fig. 8 Schematic showing the transitions of orientation and phase for symmetric DBCPs mixed with A-selective NRs ($\varphi_A = 15\%$) as the shear rate increases.

much higher than the critical shear rate, also in agreement with the previous studies, that is, for much higher shear rates, $\dot{\gamma} > \dot{\gamma}_c$, shear merely reduces the lamellar spacing.[72] For the pure NRs case shown in the lower of Fig. 8, we speculate two main effects of shear flow on NRs phase behaviors. Firstly, shear guides the orientation of NRs to rapidly turn to shear direction; secondly, shear drives NRs to disperse with the increased average inter-rod distance d_r at low rates, and with the stabilized d_r at high rates. For the DBCPs/NRs case shown in the middle of Fig. 8, the final orientations and morphological structures of nanocomposites depend on the competition between the two former phase behaviors. At low shear rates from $\dot{\gamma} = 0.01$ to 0.02, both favored parallel alignment of DBCPs and well shear-oriented NRs together help the system to transform from transverse to parallel lamellae. At the range of $\dot{\gamma} = 0.03$ to 0.06, on the one hand, the copolymers trend to adopt the perpendicular lamellae with a lower potential energy; on the other hand, NRs trend to disperse within the preferential A domain. The latter is mainly responsible for phase transitions from transverse lamellar to diagonal lamellar, ribbon and even cylindrical structures. As the average inter-rod distance d_r of NRs dispersed in the preferential A domain is increased, it equivalently enhances A-chain composition f_A, and then induces the phase transitions of lamellae-to-ribbon and lamellae-to-cylinder. Conversely, at the range of $\dot{\gamma} = 0.07$ to 0.12, the dispersion of NRs is not further enlarged, and meanwhile the DBCPs still favors perpendicular lamellae with lower potential energy and lower viscosity.[40,41] However, this time the phase behaviors of DBCPs is mainly responsible for the reverse phase transitions from transverse lamellar returning to cylindrical, ribbon and diagonal lamellar structures. The perpendicular lamellae associated with shear thinning is manifested as a reduction in period spacing d_p, which tightens the dispersions of NRs, and equivalently decreases the composition f_A, and then induces the above reverse phase transitions. Finally, at high shear rates from $\dot{\gamma} = 0.13$ to 0.21, the perpendicular lamellae is dominant for the final morphology of nanocomposites, with reducing layer spacing d_p, which not only tightens the distribution of NRs but also confines the orientation freedom of NRs within the A domain, manifested as the decrease of the average NRs orientation $\langle P(\cos\theta)\rangle$ shown in Fig. 7(a). Compared to the experimental studies by Mendoza *et al.* on the behaviors of block copolymer/gold nanoparticle composites under simple shear flow,[47–49] we also find that the shear can not only guide the orientation of self-assembled structures, but also arrange the ordered distribution of NPs in polymer matrix.

In order to monitor the processes of reorientations and phase transitions under shear, we show the simulation snapshots at different times for $\dot{\gamma} = 0.01$ in Fig. 9, for $\dot{\gamma} = 0.06$ in Fig. 10, and for $\dot{\gamma} = 0.21$ in Fig. 11. These three shear rates $\dot{\gamma}$ represent weak, moderate and strong shear, corresponding to the final microphase structures as parallel lamellae, cylinder and perpendicular lamellae, respectively. In the case of the transverse-to-parallel reorientation shown in Fig. 9, it seems that first the lamellar structure is deformed but largely retained. After about 10000 timesteps, the layers as a whole gradually reorientate so as to take the parallel orientation with some defects. Finally it takes about 20000 timesteps to eliminate the defects and achieve a steady parallel lamellar structure. In other words, the reorientation is completed by a rotating and merging of the microdomains into parallel lamellae. Fig. 10 shows the phase transition from transverse lamellae to cylinder under the shear rate of $\dot{\gamma} = 0.06$. The snapshots show the layers are broken mostly and transformed to irregular structures, connected with the adjacent ones. Subsequently, at $t = 7000$, the cylinder-like structures are merged with many defects so that some adjacent structures are still connected. Over 13000 timesteps, uniform cylinders with

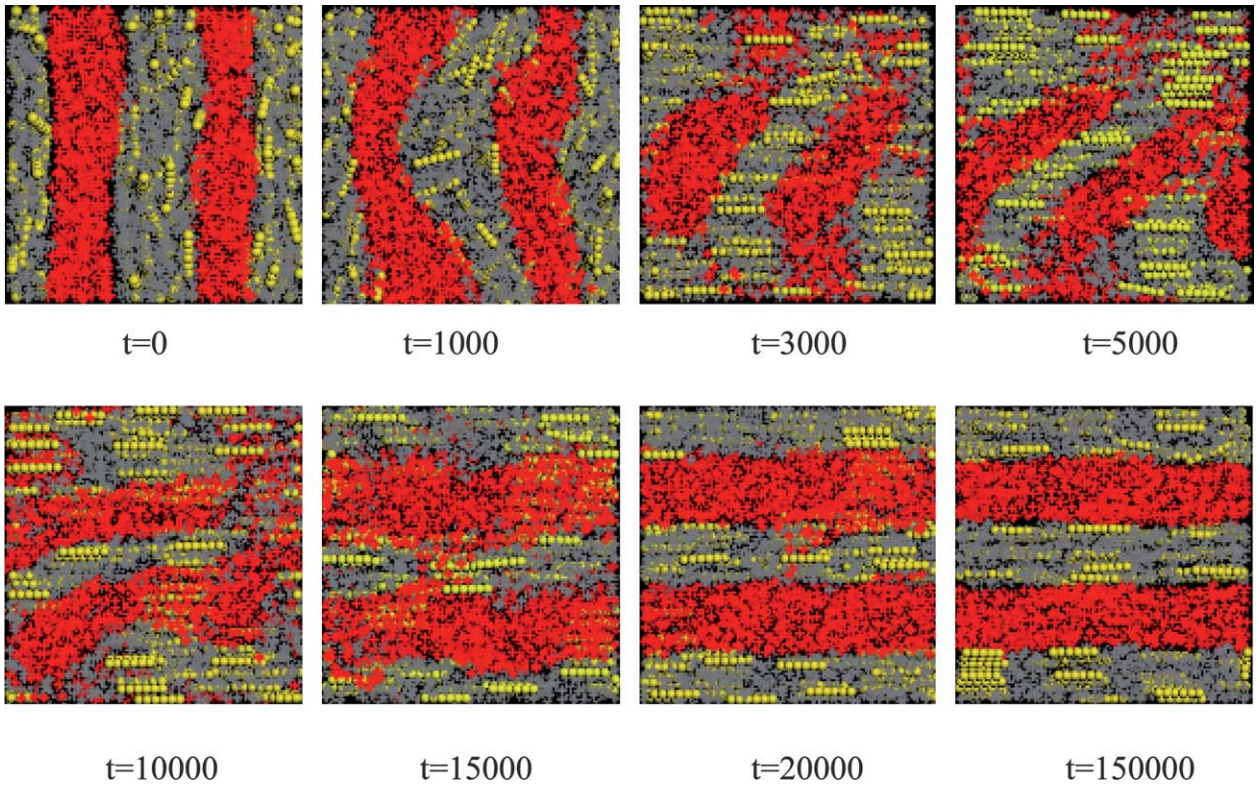

Fig. 9 Simulation snapshots for symmetric DBCPs mixed with A-selective NPs ($\varphi_A = 15\%$) at different times t corresponding to the transverse-to-parallel reorientation with a weak shear of $\dot{\gamma} = 0.01$. Here the view is perpendicular to the shear direction.

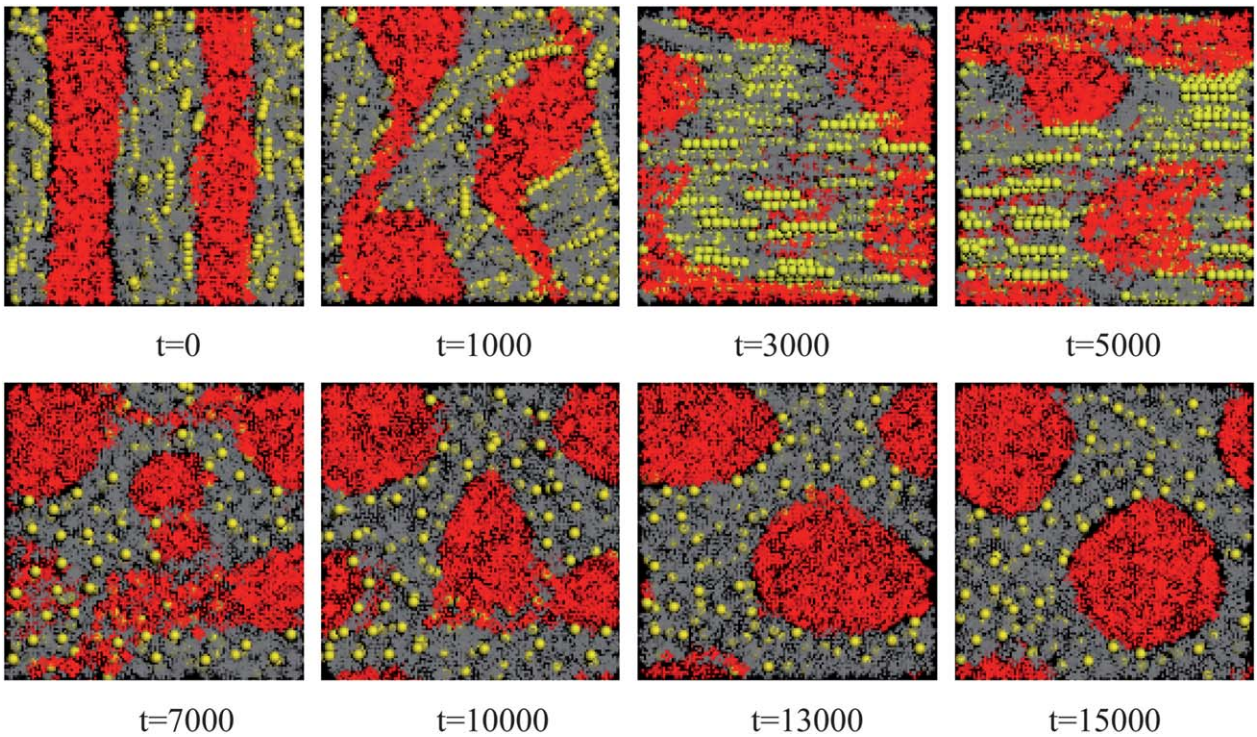

Fig. 10 Simulation snapshots for symmetric DBCPs mixed with A-selective NPs ($\varphi_A = 15\%$) at different times t corresponding to the transverse-to-cylindrical phase transition with a moderate shear of $\dot{\gamma} = 0.06$. The upper view is perpendicular to the shear direction, while the lower view is parallel to the shear direction.

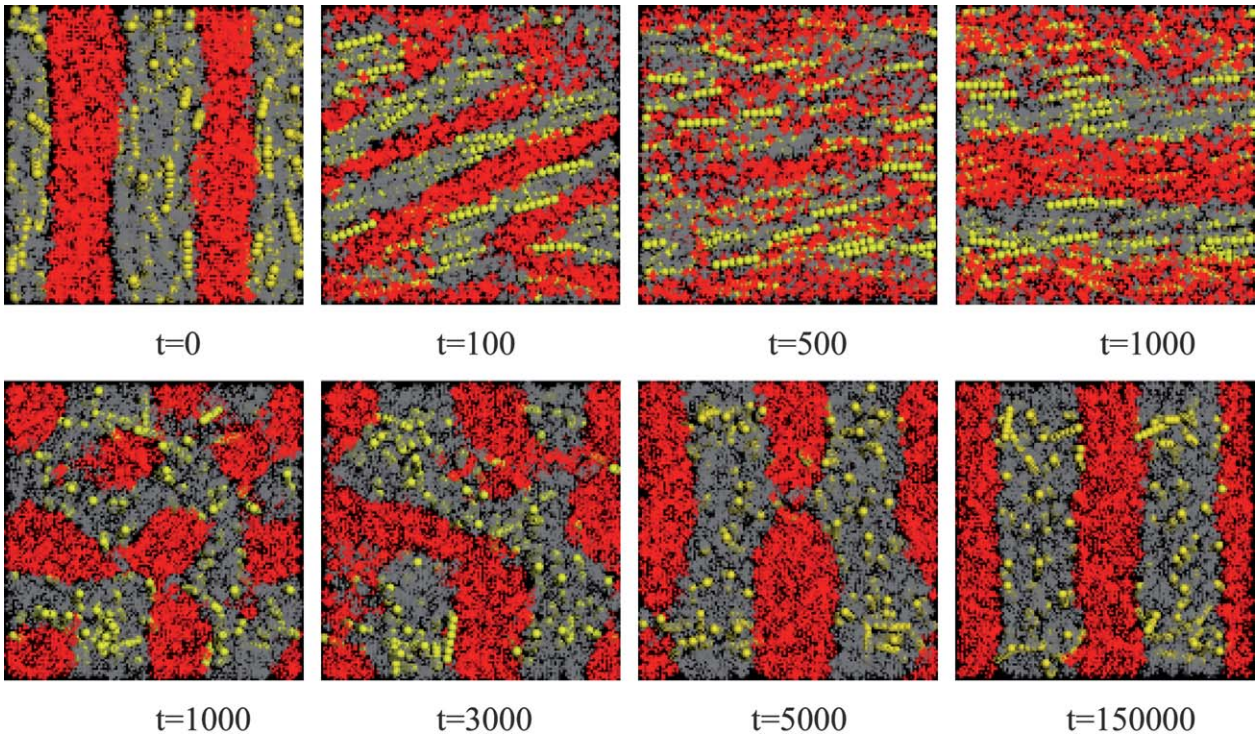

Fig. 11 Simulation snapshots for symmetric DBCPs mixed with A-selective NPs ($\varphi_A = 15\%$) at different times t corresponding to the transverse-to-perpendicular reorientation with a strong shear of $\dot{\gamma} = 0.21$. The upper view is perpendicular to the shear direction, while the lower view is parallel to the shear direction.

long-range order are observed. In the case of a transverse-to-perpendicular reorientation shown in Fig. 11, initially, the strong shear flow destroys the lamellar layers completely, and the layers are totally broken into many disordered microdomains. Later at $t = 1000$, the neighboring microdomains become interconnected through the combination of their local dislocations. At $t = 3000$, the lamellae reformation process and the reorientation process proceed concurrently, *i.e.*, as the thermodynamics of this system favors the lamellar structure, the microdomains begin to reform the lamellar structure and the shear flow induces the structure to take an energetically favored perpendicular lamellar orientation. As the perpendicular lamellae with some defects are set up, due to the strong shear rate, the defects become fewer quickly, and the perpendicular aligned lamellae appear at 5000 timesteps.

We calculate the order parameters for the above three systems, which is measured by the Saupe tensor:[73]

$$Q_{\alpha\beta} = \frac{3}{2}\left(\hat{r}_\alpha \hat{r}_\beta - \frac{1}{3}\delta_{\alpha\beta}\right) \quad (16)$$

Here, the characters α and β are Cartesian indices, and δ is the Kronecker symbol. The largest eigenvalue of the volume average of $Q_{\alpha\beta}$, S, is the order parameter. S is 0 in the completely disordered state, and it should be 1 if the system is perfectly aligned. Fig. 12 shows the temporal evolution of the transverse lamellae under three typical shear rates, $\dot{\gamma} = 0.01$, 0.06 and 0.21. The order parameter S of the initial transverse lamellae is around 0.30, *i.e.*, the characteristic value for lamellae. In the case of $\dot{\gamma} = 0.01$, S quickly decreases to reach its minimum of 0.12, which suggests that the systems still have some degree of order, corresponding to the layers being deformed but not destroyed completely. Then, S slowly increases, and finally is restored to the initial value, *i.e.*, 0.30. These results are consistent with structural evolution shown in Fig. 9. While the shear rate becomes larger, $\dot{\gamma} = 0.06$, S drops rapidly to its minimum, *i.e.*, 0.09, and then rises gradually to level off, *i.e.*, 0.12, which corresponds to the lamellae-to-cylinder transition process shown in Fig. 10. Under the strong shear of $\dot{\gamma} = 0.21$, S decreases in a very short time to its minimum of $S = 0.03$ and then increases to 0.3 quite fast, which corresponds to the rapid evolution into perpendicular lamellae as shown in Fig. 11. The curves in Fig. 12 all show a fast drop at the first stage, and their minimums become lower and lower on

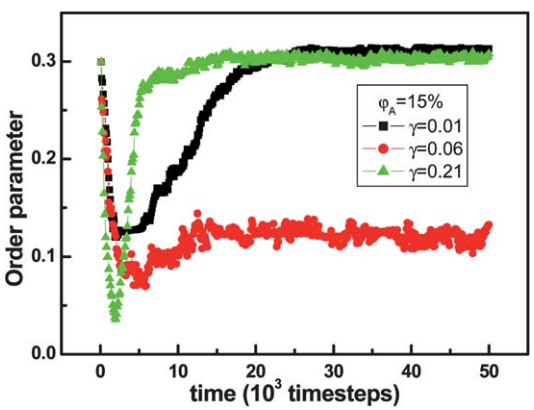

Fig. 12 Order parameter S of copolymer as a function of time for different shear rates $\dot{\gamma} = 0.01$, 0.06 and 0.21, corresponding to the transitions from transverse lamellar to parallel lamellar, cylindrical and perpendicular lamellar structure, respectively.

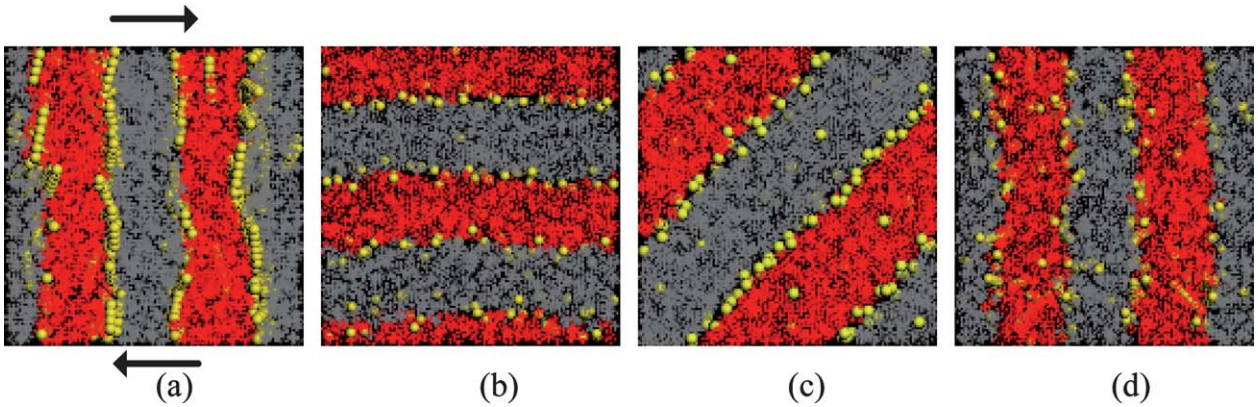

Fig. 13 Snapshots of symmetric DBCPs mixed with nonselective NRs ($\varphi_N = 15\%$) at $\dot{\gamma} = 0$, 0.01, 0.05, 0.09 in (a)–(d). The view of the initial lamellar structure in (a) is perpendicular to the shear direction, while the view in (b)–(d) is parallel to the shear direction.

increasing $\dot{\gamma}$ from 0.01 to 0.06 and to 0.21. This implies that the stronger shear rate is, the more structures are destroyed at the first stage. At the second stage, the difference between these three cases is that it takes less time to reach the final equilibrium structure, with increased shear rate, in which the nanocomposites possesses the fastest reorientation dynamics under the strongest shear of $\dot{\gamma} = 0.21$. The above results indicate that the shear flow not only can induce the reorientations and phase transitions, but also can speed up the transition process. Meanwhile, for the reorientations of lamellae taking place under weak and strong shears, respectively, we have different mechanisms: at low shear rates, the shear flow is "rotating" the layers while the layers are still intact, *i.e.*, the transverse-to-parallel reorientation is achieved *via* the rearrangement of the domains of the original zero-rate structures and layer rotation; At high shear rates, the layers experience a significant breaking-up followed by thermodynamics-driven lamellar reformation and energetically favored transverse-to-perpendicular reorientation processes. The mechanisms for reorientations is in good agreement with simulations by Rychkov *et al.* They also argued that a steady flow suppresses concentration fluctuations and a weak shear more strongly suppresses fluctuations along the shear gradient, thus stabilizing parallel orientation. In contrast, a stronger shear more strongly suppresses fluctuations along the vorticity axis, thus stabilizing perpendicular orientation.[72]

Finally, we conduct the simulations on nonselective NRs/DBCPs system with relatively high concentrations ($\phi_N = 10$ or 15%). Fig. 13 show the final snapshots with $\dot{\gamma} = 0$, 0.01, 0.05 and 0.09, corresponding to the initial transverse, parallel, diagonal and perpendicular lamellar phases, respectively. Compared to the case of $\phi_A = 15\%$, the nonselective NRs do not show any dramatic effects on the shear-induced phase transitions except the reorientations of lamellae, such as transverse-to-parallel, transverse-to-diagonal, and transverse-to-perpendicular. Having equal preference for both blocks A and B, the nonselective NRs are mainly located at the A/B interface, so the dispersion or segregation of NRs around the A/B interface domain, do not influence the composition of chains (f_{eff}) and therefore no phase transition is induced. To delineate the copolymers and NRs behavior characteristics in detail, we also plot the shear viscosity η of copolymers and the average orientation $\langle P(\cos\theta)\rangle$ of NRs shown in Fig. 14(a) and 14(b), respectively. In Fig. 14(a), the shear viscosity decreases monotonously with increasing shear rate, which corresponds to the shear thinning with no shear thickening. An evident drop in shear viscosity is seen at the shear rate of $\dot{\gamma} = 0.09$, where a transition from parallel to perpendicular takes place. Additionally, as shown in Fig. 14(b), under strong shear, each chain are tilted and stretched intensively by the shear thinning, which energetically confines the freedom of NRs orientation around the A/B interface, finally leading to

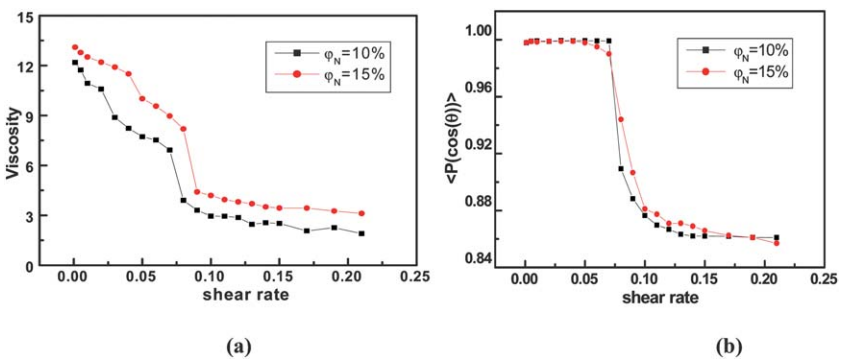

Fig. 14 Symmetric DBCPs mixed with nonselective NRs under shear. (a) The shear viscosity η as a function of shear rate $\dot{\gamma}$. (b) Average NRs orientation $\langle P(\cos\theta)\rangle$ as a function of shear rate $\dot{\gamma}$.

a decrease in the average NRs orientation $\langle P(\cos\theta)\rangle$. The observations for $\phi_N = 10\%$ are coincide with that of $\phi_N = 15\%$ shown in Fig. 14(a) and (b).

4. Conclusions

We have conducted the DPD simulations to investigate the effects of steady shear on the dynamics behaviors of symmetric DBCPs/NRs nanocomposites. For the low NRs concentration, the shear-induced lamellae adopt parallel alignment at low shear rates, while perpendicular at high shear rates, which are consistent with the pure DBCPs case. Compared to the transverse-to-perpendicular transition in the pure DBCPs system, the presence of selective NRs shifts the critical shear rate to higher values, while the presence of nonselective NRs shifts it to lower values. The shifts are caused by the equilibrium location of NRs within polymer melts. The distributions of selective and nonselective NRs within copolymer matrix still depend on the competition between entropy and enthalpy involving A, B blocks and NRs, similar to the system under equilibrium condition.

For the high concentration with selective NRs, as the shear rate increases, the initial transverse lamellae is transformed into a serial of morphologies, including parallel lamellar, diagonal lamellar, ribbon, cylindrical, ribbon, diagonal lamellar and perpendicular lamellar phases, respectively. The final morphologies of nanocomposites depend on the interplay between DBCPs and NRs under shear flow. At low shear rates, both favored parallel alignment of DBCPs and well oriented NRs together help the system to transform from transverse to parallel. With an increase of shear rates, the dispersion behavior of NRs induces an increase in the effective composition of the chains (f_{eff}), which is responsible for the phase transitions from transverse lamellae to diagonal lamellae, ribbon, and even cylindrical phases. Upon further increase of shear rates, the perpendicular alignment of DBCPs is energetically favored with the shear thinning and tightening the dispersion of NRs, which is responsible for the reverse phase transitions from transverse lamellar to cylindrical, ribbon and diagonal lamellar structures. Under stronger shear rates, the perpendicular orientation of DBCPs, with a reduction in layer width, is dominant for the final perpendicular lamellae of nanocomposites. The calculated shear viscosity, mean-squared end-to-end distance of copolymer chains, and the spatial orientation and distribution of NRs also manifest the shear-induced the reorientations and phase transitions. Moreover, enhancing the shear rate can speed up the transition process of micophase structures.

Acknowledgements

This research was financially supported by the National Natural Science Foundation of China (Nos. 20774066, 20974081, 20934004), the Program for New Century Excellent Talents in University (NCET-05-0538), the National Basic Research Program of China (No. 2005CB623800), and the Natural Science Foundation of Zhejiang Province (No. Y4080098).

References

1 H. N. W. Lekkerkerker and A. Stroobants, *Nature*, 1998, **393**, 305.
2 J. C. Loudet, P. Barois and P. Poulin, *Nature*, 2000, **407**, 611.
3 G. Peng, F. Qiu, V. V. Ginzburg, D. Jasnow and A. C. Balazs, *Science*, 2000, **288**, 1802.
4 W. A. Lopes and H. M. Jaeger, *Nature*, 2001, **414**, 735.
5 L. Leibler, *Macromolecules*, 1980, **13**, 1602.
6 C. Park, J. Yoon and E. L. Thomas, *Polymer*, 2003, **44**, 6725.
7 R. B. Thompson, V. V. Ginzburg, M. W. Matsen and A. C. Balazs, *Science*, 2001, **292**, 2469.
8 R. B Thompson, V. V. Ginzburg, M. W. Matsen and A. C. Balazs, *Macromolecules*, 2002, **35**, 1060.
9 M. R. Bockstaller and E. L. Thomas, *Phys. Rev. Lett.*, 2004, **93**, 166106–1.
10 J. Y. Lee, Z. Shou and A. C. Balazs, *Phys. Rev. Lett.*, 2003, **91**, 136103.
11 S. W. Yeh, K. H. Wei, Y. S. Sun, U. S. Jeng and K. S. Liang, *Macromolecules*, 2005, **38**, 6559.
12 B. J. Kim, J. J. Chiu, G. R. Yi, D. J. Pine and E. J. Kramer, *Adv. Mater.*, 2005, **17**, 2618.
13 M. R. Bockstaller, Y. Lapetnikov, S. Margel and E. L. Thomas, *J. Am. Chem. Soc.*, 2003, **125**, 5276.
14 J. J. Chiu, B. J. Kim, E. J. Kramer and D. J. Pine, *J. Am. Chem. Soc.*, 2005, **127**, 5036.
15 R. J. Spontak, R. Shankar, M. K. Bowman, A. S. Krishnan, M. W. Hamersky, J. Samseth, M. R. Bockstaller and K. Ø. Rasmussen, *Nano Lett.*, 2006, **6**, 2115.
16 J. Y. Lee, R. Thompson, D. Jasnow and A. C. Balazs, *Macromolecules*, 2002, **35**, 4855.
17 J. Y. Lee, R. B. Thompson, D. Jasnow and A. C. Balazs, *Phys. Rev. Lett.*, 2002, **89**, 155503-1.
18 R. B. Thompson, J. Y. Lee, D. Jasnow and A. C. Balazs, *Phys. Rev. E: Stat., Nonlinear, Soft Matter Phys.*, 2002, **66**, 031801.
19 J. Huh, V. V. Ginzburg and A. C. Balazs, *Macromolecules*, 2000, **33**, 8085.
20 L. He, L. Zhang and H. Liang, *J. Phys. Chem. B*, 2008, **112**, 4194.
21 A. J. Schultz, C. K. Hall and J. Genzer, *Macromolecules*, 2005, **38**, 3007.
22 J. Z. Jin and J. Z. Wu, *Macromolecules*, 2009, **42**, 7537.
23 S. Z. Zhang, X. S. Kou, Z. Yang, Q. H. Shi, G. D. Stucky, L. D. Sun, J. F. Wang and C. H. Yan, *Chem. Commun.*, 2007, 1816.
24 G. A. Buxton and A. C. Balazs, *J. Chem. Phys.*, 2002, **117**, 7649.
25 Q. L. Zhang, S. Gupta, T. Emrick and T. P. Russell, *J. Am. Chem. Soc.*, 2006, **128**, 3898.
26 K. Béneut, D. Constantin, P. Davidson, A. Dessombz and C. Chanéac, *Langmuir*, 2008, **24**, 8205.
27 R. D. Deshmukh, Y. Liu and R. J. Composto, *Nano Lett.*, 2007, **7**, 3662.
28 A. C. Balazs, T. Emrick and T. P. Russell, *Science*, 2006, **314**, 1107.
29 K. Chen and Y. Q. Ma, *J. Chem. Phys.*, 2002, **116**, 7783.
30 K. Chen and Y. Q. Ma, *Phys. Rev. E: Stat., Nonlinear, Soft Matter Phys.*, 2002, **65**, 041501.
31 L. He, L. Zhang and H. Liang, *Polymer*, 2010, **51**, 3303.
32 J. Feng and E. Ruckensteina, *J. Chem. Phys.*, 2004, **121**, 1609.
33 I. W. Hamley, *J. Phys.: Condens. Matter*, 2001, **13**, R643.
34 M. Pinna and A. V. Zvelindovskya, *J. Chem. Phys.*, 2006, **125**, 154905.
35 Y. R. Hong, D. H. Adamson, P. M. Chaikin and R. A. Register, *Soft Matter*, 2009, **5**, 1687.
36 J. Stasiak, M. R. Mackley, A. M. Squires, V. Castelletto, I. W. Hamley and G. D. Moggridge, *Soft Matter*, 2010, **6**, 1941.
37 S. B. Darling, *Prog. Polym. Sci.*, 2007, **32**, 1152.
38 K. Luo and Y. Yang, *Macromolecules*, 2002, **35**, 3722.
39 P. Chen and J. Viñals, *Macromolecules*, 2002, **35**, 4183.
40 B. Fraser, C. Denniston and M. H. Müser, *J. Chem. Phys.*, 2006, **124**, 104902.
41 M. Lísal and J. K. Brennan, *Langmuir*, 2007, **23**, 4809.
42 Y. R. Wang, J. H. Xu, S. E. Bechtel and K. W. Koelling, *Rheol. Acta*, 2006, **45**, 919.
43 C. Kagarise, K. W. Koelling, Y. R. Wang and S. E. Bechtel, *Rheol. Acta*, 2008, **47**, 1061.
44 T. Kairn and P. J. Daivisa, *J. Chem. Phys.*, 2005, **123**, 194905.
45 G. D. Smith, D. Bedrov, L. W. Li and O. Byutner, *J. Chem. Phys.*, 2002, **117**, 9478.
46 V. Kalra, F. Escobedo and Y. L. Jooa, *J. Chem. Phys.*, 2010, **132**, 024901.
47 C. Mendoza, T. Pietsch, N. Gindy and A. Fahmi, *Adv. Mater.*, 2008, **20**, 1179.

48 C. Mendoza, T. Pietsch, J. S. Gutmann, D. Jehnichen, N. Gindy and A. Fahmi, *Macromolecules*, 2009, **42**, 1203.
49 C. Mendoza, N. Gindy, J. S. Gutmann, A. Frömsdorf, S. Förster and A. Fahmi, *Langmuir*, 2009, **25**, 9571.
50 V. Kalra, S. Mendez, F. Escobedo and Y. L. Jooa, *J. Chem. Phys.*, 2008, **128**, 164909.
51 V. Kalra and Y. L. Jooa, *J. Chem. Phys.*, 2009, **131**, 214904.
52 L. T. Yan, N. Popp, S. K. Ghosh and A. Böker, *ACS Nano*, 2010, **4**, 913.
53 R. B. Thompson, K. Ø. Rasmussen and T. Lookman, *Nano Lett.*, 2004, **4**, 2455, 55.
54 P. J. Hoogerbrugge and J. M. V. A. Koelman, *Europhys. Lett.*, 1992, **19**, 155.
55 R. D. Groot and T. J. Madden, *J. Chem. Phys.*, 1998, **108**, 8713.
56 B. A. AlSunaidi, W. K. den Otter and J. H. R. Clarke, *Philos. Trans. R. Soc. London, Ser. A*, 2004, **362**, 1773.
57 M. J. A. Hore and M. Laradji, *J. Chem. Phys.*, 2008, **128**, 054901.
58 L. L. He, L. X. Zhang, Y. S. Ye and L. J. Liang, *J. Phys. Chem. B*, 2010, **114**, 7461.
59 C. P. Li, S. W. Yeh, H. C. Chang, J. Y. Huang and K. H. Wei, *Small*, 2006, **2**, 359.
60 M. R. Hammond, H. Dietsch, O. Pravaz and P. Schurtenberger, *Macromolecules*, 2010, **43**, 8340.
61 R. D. Groot and P. B. Warren, *J. Chem. Phys.*, 1997, **107**, 4423.
62 M. P. Allen and D. J. Tildesley, *Computer Simulation of Liquids*, Clarendon Press, Oxford, 1987.
63 A. W. Lees and S. F. Edwards, *J. Phys. C: Solid State Phys.*, 1972, **5**, 1921.
64 A. K. Khandpur, S. Foerster, F. S. Bates, I. W. Hamley, A. J. Ryan, W. Bras, K. Almdal and K. Mortensen, *Macromolecules*, 1995, **28**, 8796.
65 A. Maiti, J. Wescott and G. Goldbeck-Wood, *Int. J. Nanotechnol.*, 2005, **2**, 198.
66 K. A. Koopi, M. Tirrell, F. S. Bates, K. Almdal and R. H. Colby, *J. Phys. II*, 1992, **2**, 1941.67.
67 H. Guo, *J. Chem. Phys.*, 2006, **124**, 054902.
68 J. Zipfel, P. Lindner, M. Tsianou, P. Alexandridis and W. Richtering, *Langmuir*, 1999, **15**, 2599.
69 Z. R. Chen, J. A. Kornfield, S. D. Smith, J. T. Grothaus and M. M. Satkowski, *Science*, 1997, **277**, 1248.
70 M. W. Matsen and M. Schick, *Phys. Rev. Lett.*, 1994, **72**, 2660.
71 A. Satoh, R. W. Chantrell, S. I. Kamiyama and G. N. Coverdale, *J. Colloid Interface Sci.*, 1996, **181**, 422.
72 I. Rychkov, *Macromol. Theory Simul.*, 2005, **14**, 207.
73 P. G. de Gennes and J. Prost, *The Physics of Liquid Crystals*, Clarendon Press, Oxford, 1993.

